

# Extending the sensitivity of heavy sterile neutrino searches with solar neutrino experiments

Yutao Zhu, Haoyang Fu, Wentai Luo, Shaomin Chen, Litao Yang, and Zhicai Zhang\*

*Department of Engineering Physics, Tsinghua University, Beijing 100084, China*

*Center for High Energy Physics, Tsinghua University, Beijing 100084, China and*

*Key Laboratory of Particle & Radiation Imaging (Tsinghua University), Ministry of Education, China*

(Dated: January 23, 2026)

A sensitivity study of the search for heavy sterile neutrinos ( $\nu_H$ ) in the MeV mass range using solar neutrino experiments is presented.  $\nu_H$ , with masses ranging from a few MeV up to around 15 MeV, can be produced in the Sun through  ${}^8\text{B}$  decay and subsequently decay into  $\nu_e e^+ e^-$ . Its flux and lifetime strongly depend on the mixing parameter  $|U_{eH}|^2$  and mass  $m_{\nu_H}$ . The  $\nu_H$  signal can be detected via its decay products, either the  $e^+ e^-$  pair or  $\nu_e$ , depending on whether  $\nu_H$  decays inside or outside the detector. Expected signal yields for both detection methods (detecting  $e^+ e^-$  or  $\nu_e$  signal) are presented across the full  $|U_{eH}|^2$  and  $m_{\nu_H}$  parameter space. These two methods are found to be complementary in different regions of the  $|U_{eH}|^2$  and  $m_{\nu_H}$  phase space. By combining both approaches, we anticipate observing at least a handful of signal events across most of the parameter space of  $10^{-6} < |U_{eH}|^2 < 1$  and  $2 \text{ MeV} < m_{\nu_H} < 14 \text{ MeV}$ , assuming a 500-ton solar neutrino experiment operating for one year. Key variables, such as the energy spectra and opening angle of  $\nu_e$  or  $e^+ e^-$  and the solar angle of  $\nu_e$  and its scattered electron, are also discussed to help distinguish signal from major backgrounds, such as solar neutrino events.

Keywords: Heavy Sterile Neutrino, Solar Neutrino Experiments, Beyond Standard Model

## I. INTRODUCTION

The observation of neutrino flavor oscillations implies non-zero neutrino masses, marking one of the most significant discoveries in particle physics in the last few decades, as it lies beyond the predictions of the Standard Model of particle physics (SM). Precisely determining neutrino masses and exploring new physics models to explain their non-zero values will remain a central focus of particle physics research in the coming decades.

Theoretically, only left-handed neutrinos were introduced in the SM at the time when the SM was established, as right-handed neutrinos were thought to be unnecessary and would be invisible (or "sterile," meaning no weak or electromagnetic interactions). Due to the absence of right-handed neutrinos, neutrinos are unable to acquire mass from Yukawa couplings as other fermions do; therefore, the SM predicts that all neutrinos are massless. Experimentally, it is found that neutrino masses are not only non-zero but also exceptionally small: direct measurements from  $\beta$  decay experiments [1] and indirect constraints from Cosmological surveys [2, 3] both give an upper limit on the neutrino mass below 0.5 eV, which is more than six orders of magnitude smaller than the masses of other fermions in SM.

To explain the non-zero mass of neutrinos, new ingredients must be added to the SM, which can be either new particles, new symmetries, or other extensions. Among many neutrino mass models, one convenient way is to add right-handed neutrinos to the SM. With right-handed neutrinos, neutrino masses can arise in various ways, such

as Dirac masses as other fermions in the SM, or Majorana masses in the type-I seesaw mechanism [4–6], where the former would require extremely small Yukawa couplings (less than  $10^{-12}$ ) to explain the observed small neutrino masses, while the latter allows for larger couplings by introducing heavy sterile neutrinos that effectively suppress active neutrino masses.

Although sterile neutrinos with extremely large masses (much larger than weak scale) are preferable to bring neutrino Yukawa couplings to a similar level as for other fermions in SM, heavy sterile neutrinos with mass in the range from eV to TeV are also appealing in many aspects. Besides being accessible to a wide range of experiments, they can also address other puzzles in particle physics, such as the nature of dark matter [7] and the mechanism of leptogenesis [8].

In the type-I seesaw model, the mixing between active neutrino  $\nu_\alpha$  and sterile neutrino  $\nu_H$ ,  $|U_{\alpha H}|^2$ , is approximately the ratio of the active and sterile neutrino mass,  $m_{\nu_\alpha}/m_{\nu_H}$ . Since the mass of active neutrinos is observed to be very small (less than  $\sim 0.5$  eV), the mixing parameter would be extremely small for heavy sterile neutrinos, which means very tiny production rates of sterile neutrinos with usual neutrino sources (solar, reactor, accelerator, etc.), especially in the MeV and above range. Some variants of the seesaw model, however, can make large mixing parameters possible (for example, reference [9]). As a result, searches for heavy sterile neutrinos in the eV to TeV mass range have been performed with a wide range of experiments, from collider experiments to beta decay measurements. Current results have excluded a wide range of  $|U_{\alpha H}|^2$  and  $m_{\nu_H}$  parameter space [10], but there is still an ample uncovered phase space up to the seesaw limit ( $|U_{\alpha H}|^2 \sim m_{\nu_\alpha}/m_{\nu_H}$ ). The purpose of this paper is to discuss methods to further extend the sensitiv-

\* Correspondence: zhicaizhang@tsinghua.edu.cn

ity in the MeV mass range with solar neutrino detectors (currently in operation or under construction).

## II. PRODUCTION AND DECAY OF HEAVY STERILE NEUTRINO

Heavy sterile neutrinos ( $\nu_H$ ) with masses of a few MeV can be produced from solar neutrinos ( $\nu_e$ ) through active-sterile neutrino mixing, for example, from  ${}^8\text{B}$  solar neutrino as a primary source:

$${}^8\text{B} \rightarrow {}^8\text{Be}^* + e^+ + \nu_e \rightarrow {}^8\text{Be}^* + e^+ + \nu_H \quad (1)$$

The flux of  $\nu_H$  from such decay chain is proportional to the  ${}^8\text{B}$  solar neutrino flux and the mixing parameter  $|U_{\alpha H}|^2$ , scaled by a mass-dependent phase-space factor:

$$\Phi_{\nu_H}(E) = |U_{eH}|^2 \sqrt{1 - \left(\frac{m_{\nu_H}}{E}\right)^2} \Phi_{{}^8\text{B}}(E), \quad (2)$$

where  $m_{\nu_H}$  and  $E$  are the mass and energy of the heavy sterile neutrino, respectively. Using Eq. 2 and  ${}^8\text{B}$  solar neutrino spectrum from [11], we can plot the energy spectra of  $\nu_H$  from  ${}^8\text{B}$  decay for different  $\nu_H$  masses, as shown in Fig. 1.

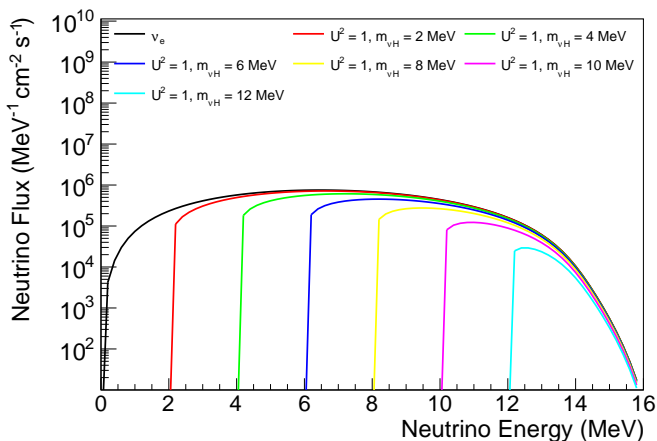


FIG. 1: Energy spectra of  $\nu_H$  with different masses emitted from  ${}^8\text{B}$  decay in the Sun. The spectra are based on the  ${}^8\text{B}$  left-handed solar neutrino spectrum ( $\nu_e$  in the plot, taken from [11]) and are suppressed by the mixing parameter  $|U_{eH}|^2$  and the phase-space factor according to Eq. 2, where  $|U_{eH}|^2 = 1.0$  in the spectra shown in this plot.

The goal of this work is to explore possible methods to extend the discovery potential of such heavy sterile neutrinos with mixing parameter  $|U_{eH}|^2$  much smaller than 1, getting as close as possible to the seesaw limit (for MeV mass, the seesaw limit is around  $|U_{eH}|^2 \sim 10^{-7}$  or even smaller). With such a small mixing parameter,

the deficit of  ${}^8\text{B}$  solar neutrino due to mixing to sterile neutrino will be practically invisible to a solar neutrino detector of a few hundred tons (which has a daily  ${}^8\text{B}$  solar neutrino event rate of about one). As a result, the rest of this paper will discuss the direct search for heavy sterile neutrinos from  ${}^8\text{B}$  decay.

For  $\nu_H$  with a mass heavier than two times the electron mass, they can decay into an  $e^+e^-$  pair plus a left-handed neutrino  $\nu_e$ . The Feynman diagram for the production of a heavy sterile neutrino from  ${}^8\text{B}$  solar neutrino and its subsequent decay can be seen in Fig. 2.

In addition to  $\nu_H \rightarrow e^+e^-\nu_e$  decay,  $\nu_H$  can also decay into three neutrinos ( $\nu_e$ ) via Z boson exchange, as well as radiatively decay into  $\nu_e + \gamma$  through a W and lepton loop. The width of  $\nu_H \rightarrow \nu_e + \gamma$  decay is negligible compared to  $e^+e^-\nu_e$  or three-neutrino decay. Calculating the matrix element for  $\nu_H$  decaying to three active neutrinos is straightforward, and after phase space integration, we obtain the width in the following form:

$$\Gamma_{3\nu_e} = \frac{G_F^2}{192\pi^3} m_{\nu_H}^5 |U_{eH}|^2 \quad (3)$$

The width of  $\nu_H \rightarrow e^+e^-\nu_e$  is similar to that of  $\nu_H \rightarrow 3\nu_e$ , with minor differences due to the mixed vector and vector-axial terms and the non-negligible electron mass. The exact value of  $\Gamma_{e^+e^-\nu_e}$  can be found in [12]. For  $\nu_H$  with sufficiently large mass ( $m_{\nu_H} \gg m_e$ ), the ratio of  $\Gamma_{e^+e^-\nu_e}$  to  $\Gamma_{3\nu_e}$  is approximately:

$$\frac{\Gamma_{e^+e^-\nu_e}}{\Gamma_{3\nu_e}} \approx \frac{1}{4} (1 - 4\sin^2\theta_w + 8\sin^2\theta_w) \approx 0.6 \quad (4)$$

From the width calculations above, we can determine the proper lifetime of  $\nu_H$  decay as a function of its mass and the mixing parameter  $|U_{eH}|^2$ , as shown in Fig. 3. It can be seen that  $\nu_H$  with small mass and small mixing parameter can have an extremely long lifetime, which is evident from Eq. 3. For the lower left corner (small mass and small mixing parameter), only a small fraction of  $\nu_H$  decays before reaching our detector on Earth; while for the upper right corner (large mass and large mixing parameter), most  $\nu_H$  decays within Earth's orbit.

Since  $\nu_H$  itself doesn't produce detectable signals in most traditional neutrino detectors (except those designed to detect extremely weak signals like coherent elastic neutrino-nucleus scattering, as reported in [13]), direct searches for  $\nu_H$  typically rely on detecting its decay products. These could be either the  $e^+e^-$  pair or the  $\nu_e$  shown in Fig. 2, as illustrated in Fig. 4:

- **Method 1:** If  $\nu_H$  decays inside the detector, we can search for the  $e^+e^-$  signal event within the detector.
- **Method 2:** If  $\nu_H$  decays before reaching the detector, the detectable signal would be a  $\nu_e$  event in our detector.

The remainder of this paper explores both methods and discusses their complementary sensitivity across the full phase space of  $m_{\nu_H}$  and  $|U_{eH}|^2$ .

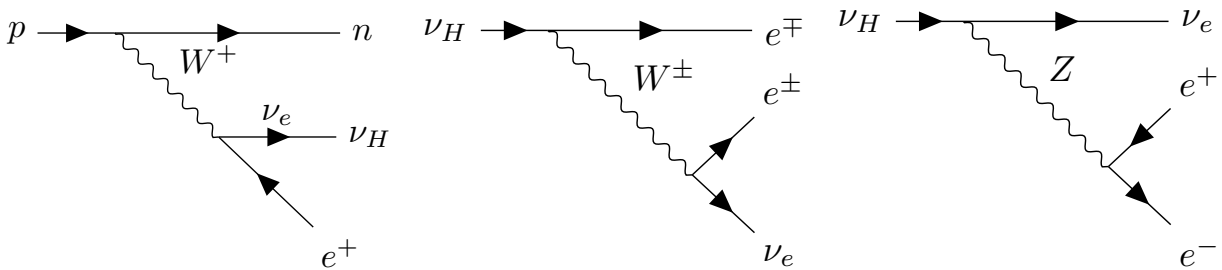


FIG. 2: Feynman diagrams of  $\nu_H$  production from solar  ${}^8\text{B}$  decay and its decay  $\nu_H \rightarrow e^+e^-\nu_e$  via  $W^\pm$  or  $Z$  boson exchange.

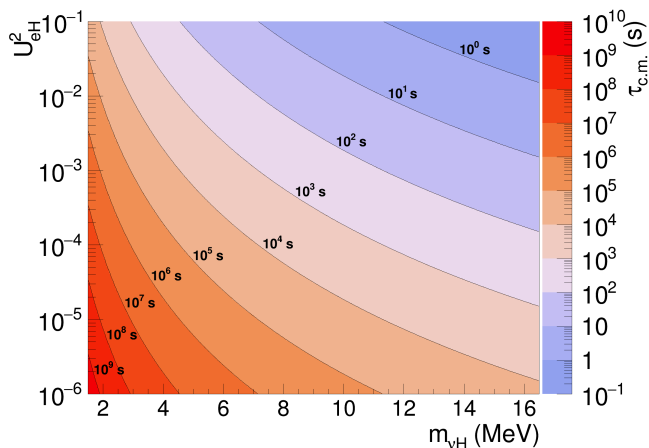
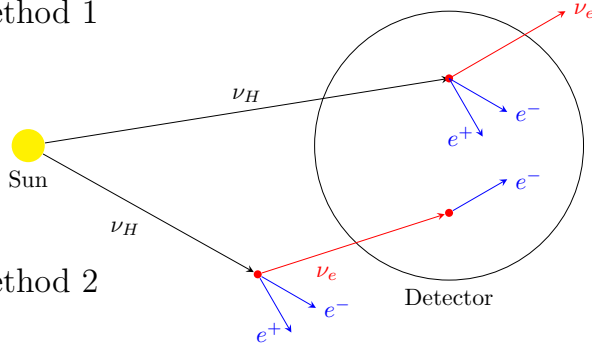


FIG. 3: Proper lifetime ( $\tau_{c.m.} = 1/\Gamma_{\text{total}}$ ) of  $\nu_H$  as a function of mass  $m_{\nu_H}$  and mixing parameter  $|U_{eH}|^2$ .

#### Method 1



#### Method 2

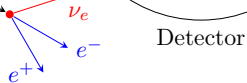


FIG. 4: Two detection Methods for heavy sterile neutrinos: (1)  $e^+e^-$  pair detection from  $\nu_H$  decays occurring inside the detector, and (2)  $\nu_e$  detection from  $\nu_H$  decays occurring outside the detector.

### III. METHOD 1: SEARCH FOR $\nu_H$ BY $e^+e^-$ SIGNAL

To estimate the sensitivity of  $\nu_H$  searches using the  $e^+e^-$  signal from its decay, we calculate and present the event rates for both signal and major background events,

along with the distribution of a key discriminating variable—the total energy deposition spectrum—across the entire  $m_{\nu_H}-|U_{eH}|^2$  parameter space under investigation.

The signal event rate can be estimated by calculating the  $\nu_H$  decay rate within the detector. For  $\nu_H$  with production rate  $R_0$  at the Sun (source), lifetime  $\tau$ , Sun-to-Earth time of flight  $t$ , time of flight inside the detector  $dt$ , and detector solid angle  $d\Omega$  relative to the Sun, the  $\nu_H$  decay rate inside the detector is given by:

$$R = R_0 \frac{d\Omega}{4\pi} \frac{dt}{\tau} \exp\left(-\frac{t}{\tau}\right) \quad (5)$$

To analyze the rate variation across different regions of the  $m_{\nu_H}-|U_{eH}|^2$  parameter space, we can treat  $\tau$  as the primary variable of change since  $t$  and  $dt$  remain relatively constant for different  $m_{\nu_H}$  and  $|U_{eH}|^2$  values. By taking the derivative  $dR/d\tau$  of Eq. 5, we find that  $R$  increases with  $\tau$  until  $\tau = t$  (approximately 500 seconds in most cases), after which  $R$  decreases as  $\tau$  continues to increase.

Combining this observation with the lifetime distribution shown in Fig. 3 and the source rate ( $R_0$ ) from Eq. 2, we can conclude:

1. The ratio  $R/R_0$  (total signal efficiency) peaks near the  $\tau = 500$  s contour in Fig. 3 and reaches minima at both corners (lower left and upper right).
2. According to Eq. 2,  $R_0$  is maximized in the upper left corner of Fig. 3 and minimized in the lower right corner.
3. Consequently, the signal event rate  $R$  contour lines in the  $|U_{eH}|^2$  vs.  $m_{\nu_H}$  plane resemble a crest aligned with the  $\tau = 500$  s contour (approximately diagonal in Fig. 3), with the maximum at the upper left corner and minimum at the lower right corner.

The exact values of  $R$  in Eq. 5 can be obtained by substituting  $R_0$  with the total flux from Eq. 2 and calculating the time of flight ( $t$  or  $dt$ ) using:

$$t = \frac{m_{\nu_H}}{E_{\nu_H}} \frac{D}{\beta c} \quad (6)$$

where  $D$  represents the travel distance (Sun-Earth distance for  $t$  or detector size for  $dt$ ). For a 500-ton spherical detector on Earth, we calculated the expected  $e^+e^-$  signal event rates from  $\nu_H$  decay across various  $m_{\nu_H}$  and  $|U_{eH}|^2$  values, as summarized in table I. These results are visualized in the top panel of Fig. 5, showing the expected crest-like contour pattern in the signal rate distribution.

The primary background for  $e^+e^-$  signals from  $\nu_H$  decays in solar neutrino detectors comes from electrons produced through elastic scattering of solar neutrinos with detector materials. The key distinction between  $\nu_H$  signals and solar neutrino backgrounds lies in their final states:  $\nu_H$  decays produce  $e^+e^-$  pairs, while background events generate single electrons.

For Cherenkov detectors,  $e^+e^-$  pairs can potentially be distinguished from single electrons when their opening angle is sufficiently large. Scintillation detectors, however, must rely on differences in total deposited energy spectra for signal-background separation. Advanced slow scintillation detectors with directional sensitivity [14] can leverage both energy spectra and opening angle information to optimize signal-to-background ratios.

We now calculate the expected energy spectrum of  $e^+e^-$  pairs from  $\nu_H$  decays and compare it with solar neutrino background spectra. The differential width for  $\nu_H \rightarrow e^+e^-\nu_e$  decay can be found in [15], which takes the form:

$$\frac{d\Gamma}{dE d\cos\theta} = \Gamma_{\text{total}}(f_1 + \zeta|\vec{P}|f_S \cos\theta), \quad (7)$$

where  $E$  and  $\theta$  represent the energy and emission angle of  $\nu_e$  in the  $\nu_H$  rest frame;  $\Gamma_{\text{total}}$  is the total decay width;  $f_1$  and  $f_S$  are functions of  $m_{\nu_H}$  and  $E$ ;  $|\vec{P}| \approx \beta$  denotes the  $\nu_H$  polarization; and  $\zeta = +1$  ( $-1$ ) for  $\nu_H$  ( $\bar{\nu}_H$ ).

Using the  $\nu_e$  energy spectrum from Eq. 7 in the  $\nu_H$  rest frame, we compute the total  $e^+e^-$  energy spectrum in the laboratory frame. The  $e^+e^-$  spectral shape varies with  $m_{\nu_H}$ , as shown in the bottom panel of Fig. 5. This plot compares  $e^+e^-$  spectra from  $\nu_H$  decays (normalized to rates in a 500-ton Earth-based detector) with electron spectra from  ${}^8\text{B}$  solar neutrino elastic scattering. Distinct spectral peaks emerge at the tail of the background spectrum for most  $\nu_H$  masses, suggesting that precise energy measurements in scintillation detectors should enable excellent signal-background discrimination through spectral fitting.

Combining the information from the top and bottom plots of Fig. 5, we expect to observe at least a handful of  $\nu_H \rightarrow e^+e^-\nu_e$  events by detection of  $e^+e^-$  inside the detector for most regions where  $|U_{eH}|^2 > 10^{-6}$  and  $2 \text{ MeV} < m_{\nu_H} < 14 \text{ MeV}$ . Using the  $e^+e^-$  total energy spectrum, the Borexino experiment has excluded some phase space in the above region of  $|U_{eH}|^2$  and  $m_{\nu_H}$  using 446 days of Borexino data [16]. Future solar neutrino observatories with larger central volumes and direction measurement capabilities—and therefore better separation of  $e^+e^-$  from single electron events—such as the Jinping Neutrino Experiment (JNE) [14, 17], could further extend the sensitivity to  $\nu_H$  in these regions.

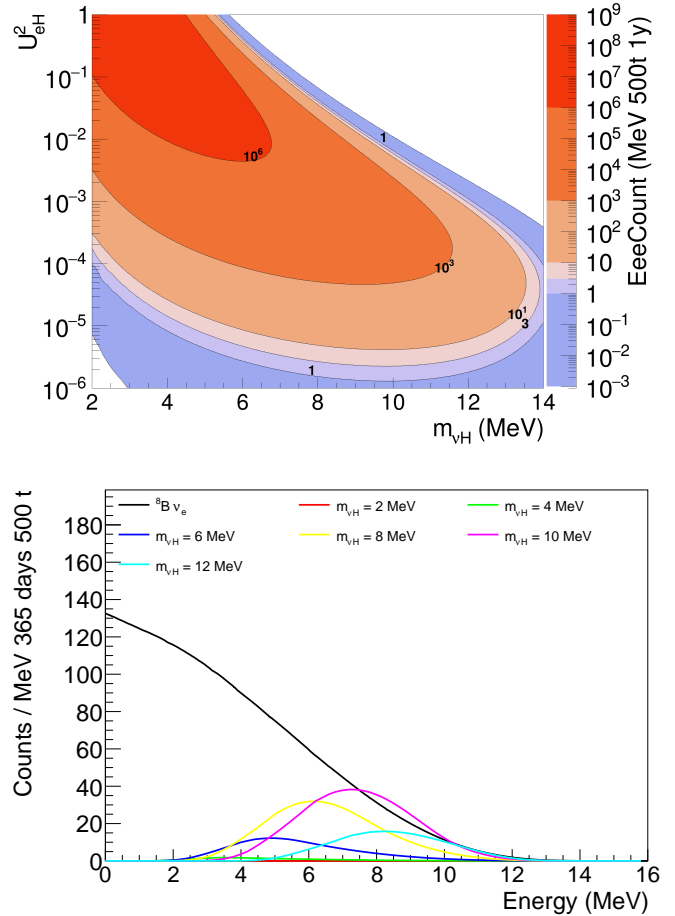


FIG. 5: Top: The count rate (per year) of  $e^+e^-$  signal from  $\nu_H$  decay inside a 500-ton detector on Earth, as a function of  $m_{\nu_H}$  and  $|U_{eH}|^2$ . Bottom: The energy spectrum of  $e^+e^-$  signal from  $\nu_H$  decay, along with the energy spectrum of the major background (scattered electron in the detector from solar  ${}^8\text{B}$  neutrino).

Different values of  $\nu_H$  mass are shown, with  $|U_{eH}|^2 = 10^{-5}$ .

The uncovered regions in the phase space are the lower-left and upper-right corners of  $|U_{eH}|^2$  and  $m_{\nu_H}$ , as shown in Fig. 5, where  $\nu_H$  is either too short-lived or too long-lived, leading to insufficient  $\nu_H$  decays inside the detector. To cover those regions, one must search for  $\nu_H$  that decays outside the detector, for which the only method is to detect the  $\nu_e$  from  $\nu_H$  decay, which will be discussed in the next section.

Furthermore, to obtain the energy and angular distributions of the decay products, we employ MadGraph aMC@NLO [18] to generate decay events in the rest frame of the heavy neutrino ( $\nu_H \rightarrow \nu_e e^+ e^-$ ). These events are subsequently boosted to the laboratory frame by sampling from the predicted  $\nu_H$  energy spectrum (Fig. 1). As shown in Fig. 6, for the majority of events, the opening angle of the  $e^+e^-$  pair is sufficiently large

$ U_{eH} ^2 \backslash M_{\nu_H}$	2	4	6	8	10	12
$10^{-1}$	$9.2 \times 10^5$	$3.6 \times 10^7$	$2.3 \times 10^5$	0	0	0
$10^{-2}$	$9.5 \times 10^3$	$1.2 \times 10^6$	$2.3 \times 10^6$	$3.4 \times 10^4$	0	0
$10^{-3}$	96.6	$1.41 \times 10^4$	$1.0 \times 10^5$	$1.2 \times 10^5$	$8.8 \times 10^3$	2.1
$10^{-4}$	1.1	$1.4 \times 10^2$	$1.3 \times 10^3$	$3.5 \times 10^3$	$3.1 \times 10^3$	$4.3 \times 10^2$
$10^{-5}$	0	1.5	13.5	41.5	55.4	24.6
$10^{-6}$	0	0.02	0.1	0.4	0.6	0.3

TABLE I: Expected event rate (per year) of  $e^+e^-$  pairs from  $\nu_H \rightarrow \nu_e e^+e^-$  decays occurring within the detector, shown for different mixing parameters  $|U_{eH}|^2$  and  $\nu_H$  masses, assuming a 500-ton Earth-based detector.

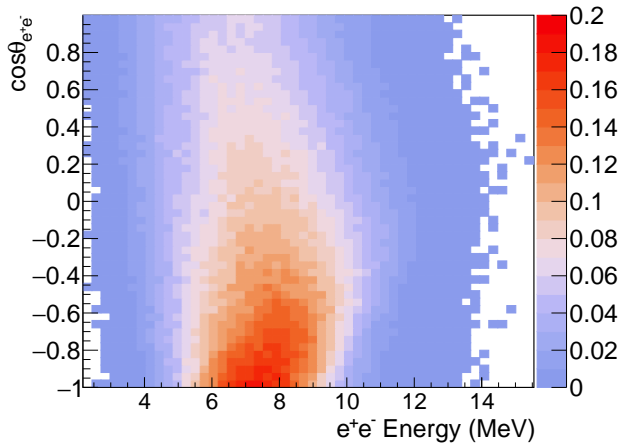
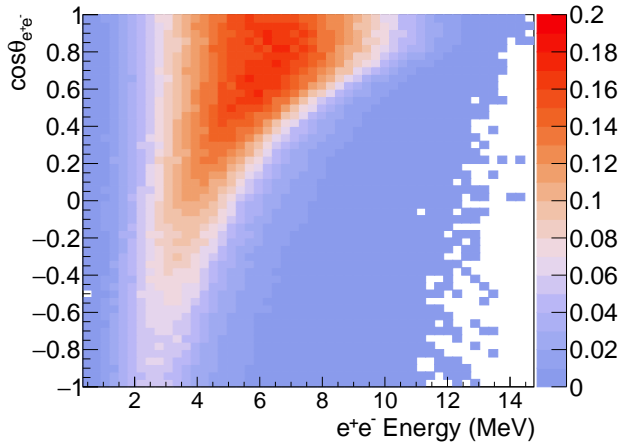


FIG. 6: Distribution of opening angle and energy of  $e^+e^-$  pairs from  $\nu_H$  decay with  $|U_{eH}|^2 = 10^{-5}$ . Top:  $m_{\nu_H} = 4$  MeV; Bottom:  $m_{\nu_H} = 10$  MeV

to allow these pairs to be distinguished from background events containing single electrons. Moreover, as the mass of the right-handed neutrino increases, the proportion of events with a larger opening angle also increases.

#### IV. METHOD 2: SEARCH FOR $\nu_H$ BY $\nu_e$ SIGNAL

For regions of  $|U_{eH}|^2$  and  $m_{\nu_H}$  where the  $\nu_H$  is too short-lived, the majority of  $\nu_H$  will decay before they reach the Earth orbit. Among the decay products, the only particle that can reach our detector on Earth is the active neutrino  $\nu_e$ . The  $\nu_e$  from  $\nu_H$  decay is similar to solar neutrinos, making it challenging to distinguish this signal from the solar neutrino background. No such search has been performed with existing solar neutrino detectors worldwide.

This paper explores two variables to differentiate  $\nu_e$  from  $\nu_H$  decay and solar neutrino background: the  $\nu_e$  energy and direction. The signal  $\nu_e$  is from  $\nu_H$  decay, and  $\nu_H$  itself is from a solar neutrino by active-sterile mixing; therefore, the energy of the signal  $\nu_e$  should be significantly lower than the original solar neutrino energy. As for the  $\nu_e$  direction, the solar neutrino we detect on Earth always comes from the Sun, but the  $\nu_H$  can decay anywhere in space and generate a  $\nu_e$  that travels to the Earth. Consequently, the angle between the  $\nu_e$  direction and the Sun-Earth line ( $\theta_{\text{Sun}}$ ) should be different for the signal and background.

The calculation of the energy and angular distribution of  $\nu_e$  from  $\nu_H$  that reaches the detector on Earth begins with the energy and angular distribution of all emitted  $\nu_e$  from  $\nu_H$ , as shown in Eq. 7. From Eq. 7, we just need to integrate over all  $\nu_H$  decay points in space and all  $\nu_e$  emission angles to collect all  $\nu_e$  that can reach our detector on Earth. Fig. 7 shows two typical situations of the decay of  $\nu_H$  with  $\nu_e$  entering the detector on Earth, where the  $\nu_H$  can either decay inside or outside the Earth's orbit. Two angles are defined and illustrated in Fig. 7:

1.  $\nu_e$  emission angle  $\phi_{\text{decay}}$ : angle between  $\nu_H$  and  $\nu_e$  direction. This angle is the same as the angle  $\theta$  in Eq. 7 (except that  $\theta$  in Eq. 7 is in  $\nu_H$  rest frame, and  $\phi_{\text{decay}}$  is in lab frame).
2.  $\nu_e$  solar angle  $\theta_{\text{Sun}}$ : angle between  $\nu_e$  direction and the Sun-Earth line.

The 3-dimensional integration over all space can be simplified to a 1-dimensional integration when calculating the energy and  $\theta_{\text{Sun}}$  distributions of all  $\nu_e$  that reach our detector on Earth. The simplification is based on

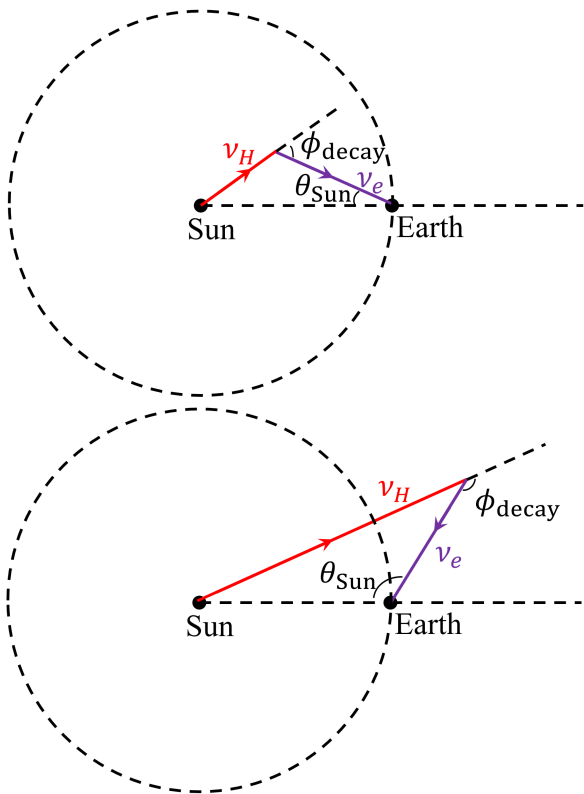


FIG. 7: Definition of angles  $\phi_{decay}$  (emission angle) and  $\theta_{Sun}$  (solar angle) for  $\nu_H$  decay in flight and then the decay product  $\nu_e$  reaches the detector on earth. Different Methods of  $\nu_H$  decays are shown:  $\nu_H$  decay inside Earth orbit (top plot), and  $\nu_H$  decay outside Earth orbit (bottom plot).

the fact that all detectors placed on any point on the spherical surface  $S$  with the Sun as the center and the Sun-Earth distance as the radius should have the same energy and  $\theta_{Sun}$  distributions of  $\nu_e$ . Therefore, we only need to consider decay vertices along a straight line from the Sun to infinity, integrating over decays where  $\nu_e$  intersects with surface  $S$ . The energy distribution of these intersecting  $\nu_e$  corresponds directly to our signal's energy spectrum for an Earth-based detector. Additionally, the angle between the direction of  $\nu_e$  and the line from the Sun to their intersection gives the desired  $\theta_{Sun}$  distribution.

Fig. 8 shows the energy spectra of  $\nu_e$ 's from  $\nu_H$  decay that reach Earth's detector. As expected, the signal  $\nu_e$  from this decay is much softer than the background  ${}^8\text{B}$  solar neutrino, peaking below 5 MeV. Distinguishing these low-energy  $\nu_e$  from background solar neutrinos is challenging, as the electron energy from the elastic scattering of  ${}^8\text{B}$  also peaks at low energies, as shown in Fig. 5. A good signal-to-background ratio will significantly enhance  $\nu_e$  detection through charged-current interactions (as proposed in [19, 20]), where the recoil energy closely correlates with the neutrino energy.

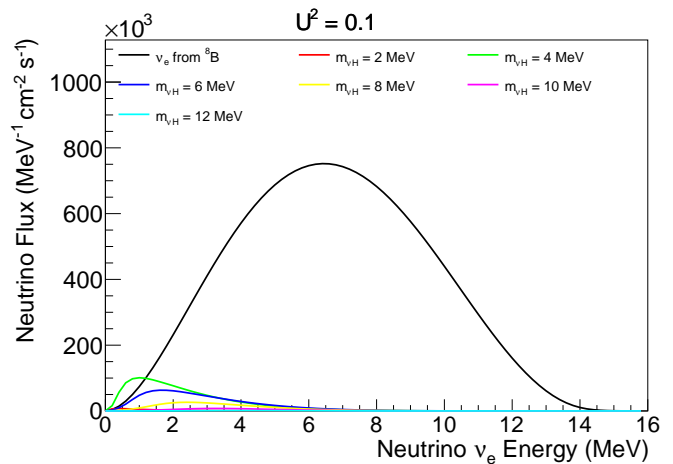


FIG. 8: Energy spectra of  $\nu_e$ 's from  $\nu_H$  decay that reach the detector on Earth for different values of  $m_{\nu_H}$  with  $|U_{eH}|^2 = 0.1$ . The plot also shows the energy spectrum of background  ${}^8\text{B}$  solar neutrino (black curve).

The solar angle  $\theta_{Sun}$  distinguishes the signal  $\nu_e$  (from  $\nu_H$  decay) from the solar neutrino background. The background solar neutrinos have a solar angle of zero since they originate from the Sun. Fig. 9 illustrates the distribution of the solar angle for signal  $\nu_e$  based on specific values of  $m_{\nu_H}$  and  $|U_{eH}|^2$ . For signal  $\nu_e$ , there is a small but significant tail with large solar angles that can exceed typical angular resolution limits (around  $25^\circ$ ) of standard detectors. The bottom plot in Fig. 9 shows that for  $|U_{eH}|^2 > 10^{-2}$ , there is a large region with at least 10% of  $\nu_e$  events having a solar angle  $\theta_{Sun} > 25^\circ$  (or  $\cos\theta_{Sun} < 0.9$ ), allowing them to be distinguished from background neutrinos by major detectors capable of direction measurement.

Considering the  $\nu_e$ -electron scattering cross section (approximately  $9.4 \times 10^{-45} \text{ cm}^2$  for  $E_{\nu_e} = 10 \text{ MeV}$ ), we can estimate the expected event count rate for detecting  $\nu_e$  signals from  $\nu_H$  decay, as shown in Fig. 10. In most of the phase space where  $|U_{eH}|^2 > 10^{-2}$ , we expect to observe at least a few  $\nu_H$  events by detecting  $\nu_e$  from its decay, using about one year of data from a 500-ton solar neutrino detector. Unlike Fig. 5, much of this phase space cannot be explored by searching for  $e^+e^-$  signals due to the short lifetime of  $\nu_H$ .

In addition, the solar angle cosine distribution of  $e^-$  from  $\nu_e$ - $e^-$  scattering is obtained and presented in Fig. 11. Based on Fig. 11, it is expected that scattered electrons with large solar angles are the low energy ones (below 2 MeV for  $\cos(\theta_{Sun}) < 0.9$ ). At such low kinetic energies, it remains challenging to utilize directional information to effectively distinguish these signals from the  ${}^8\text{B}$  solar neutrino background.

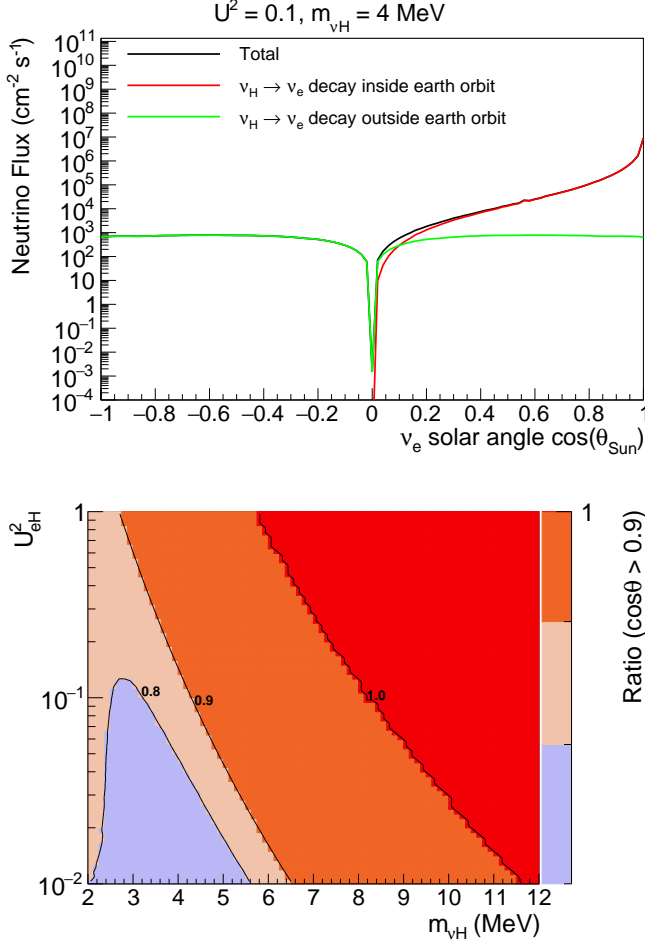


FIG. 9: Top: distribution of  $\cos \theta_{\text{Sun}}$  of  $\nu_e$  from  $\nu_H$  decay and then reach the detector on earth with  $m_{\nu_H} = 4 \text{ MeV}$  and  $|U_{eH}|^2 = 0.1$ . The distributions for  $\nu_H$  decay inside and outside Earth orbit are shown separately. Bottom: Ratio of  $\nu_e$  with  $\cos \theta_{\text{Sun}} > 0.9$  for different  $m_{\nu_H}$  and  $|U_{eH}|^2$ .

## V. SUMMARY

Solar neutrino experiments, particularly those with new designs that provide good energy and direction measurements, are promising for heavy sterile neutrino searches in the MeV mass range. In this range,  $\nu_H$  can decay into an  $e^+e^-$  pair plus an active neutrino  $\nu_e$ . This paper presents two methods based on this decay: one focuses on detecting ample  $e^+e^-$  signals from  $\nu_H$  decays with an intermediate lifetime, while the other aims to find  $\nu_e$  from short-lived  $\nu_H$  decays. The estimated signal and background event yields indicate the complementary sensitivity of both methods. Key variables to distinguish the  $\nu_H$  signal from solar neutrino events are proposed along

with their distributions. By combining these methods, it is expected to be sensitive in most of the phase space where  $|U_{eH}|^2 > 10^{-6}$  and  $2 \text{ MeV} < m_{\nu_H} < 14 \text{ MeV}$  using data from a 500-ton detector over one year.

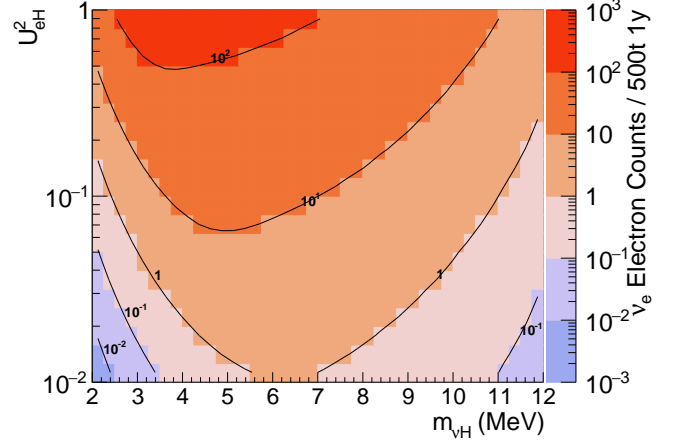


FIG. 10: Event rate of  $\nu_e$ -electron elastic scattering with a 500-ton detector for  $\nu_e$  signal from  $\nu_H$  decay.

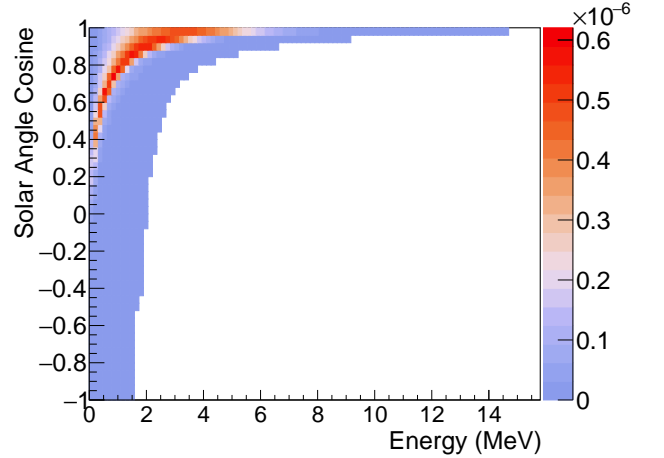


FIG. 11: Distribution of solar angle and energy of scattering electron with  $m_{\nu_H} = 4 \text{ MeV}$  and  $|U_{eH}|^2 = 0.1$ .

## ACKNOWLEDGMENTS

This work is supported by the National Key Research and Development Plan of China (Project No. 2022YFA1604700), the National Natural Science Foundation of China (Grant No. 12521007 and No. 12575108), and the Tsinghua University Initiative Scientific Research Program.

[1] Direct neutrino-mass measurement based on 259

days of KATRIN data, *Science* **388**, 180 (2025),

- arXiv:2406.13516.
- [2] DESI 2024 VI: cosmological constraints from the measurements of baryon acoustic oscillations, *Journal of Cosmology and Astroparticle Physics* **2025** (02), 021, arXiv:2404.03002.
- [3] Planck 2018 results - VI. Cosmological parameters, *A&A* **641**, A6 (2020), arXiv:1807.06209.
- [4] M. Gell-Mann, P. Ramond, and R. Slansky, Complex Spinors and Unified Theories, *Conf. Proc. C* **790927**, 315 (1979), arXiv:1306.4669 [hep-th].
- [5] T. Yanagida, Horizontal gauge symmetry and masses of neutrinos, *Conf. Proc. C* **7902131**, 95 (1979).
- [6] R. N. Mohapatra and G. Senjanović, Neutrino Mass and Spontaneous Parity Nonconservation, *Phys. Rev. Lett.* **44**, 912 (1980).
- [7] T. Asaka, S. Blanchet, and M. Shaposhnikov, The  $\nu$ MSM, dark matter and neutrino masses, *Physics Letters B* **631**, 151 (2005), arXiv:hep-ph/0503065.
- [8] E. K. Akhmedov, V. A. Rubakov, and A. Y. Smirnov, Baryogenesis via Neutrino Oscillations, *Phys. Rev. Lett.* **81**, 1359 (1998), arXiv:hep-ph/9803255.
- [9] X.-G. He, S. Oh, J. Tandean, and C.-C. Wen, Large mixing of light and heavy neutrinos in seesaw models and the LHC, *Phys. Rev. D* **80**, 073012 (2009), arXiv:0907.1607.
- [10] P. D. Bolton, F. F. Deppisch, and P. Dev, Neutrinoless double beta decay versus other probes of heavy sterile neutrinos, *Journal of High Energy Physics* **2020**, 170 (2020), arXiv:1912.03058.
- [11] J. N. Bahcall, E. Lisi, D. E. Alburger, L. De Braeckeleer, S. J. Freedman, and J. Napolitano, Standard Neutrino Spectrum from B 8 Decay, *Physical Review C* **54**, 411 (1996).
- [12] D. Gorbunov and M. Shaposhnikov, How to Find Neutral Leptons of the  $\nu$ MSM?, *Journal of High Energy Physics* **2007**, 015 (2007).
- [13] First Indication of Solar  $^8\text{B}$  Neutrinos via Coherent Elastic Neutrino-Nucleus Scattering with XENONnT, *Phys. Rev. Lett.* **133**, 191002 (2024).
- [14] W. Luo, Q. Liu, Y. Zheng, Z. Wang, and S. Chen, Reconstruction algorithm for a novel Cherenkov scintillation detector, *Journal of Instrumentation* **18** (02), P02004, arXiv:2209.13772.
- [15] R. E. Shrock, General Theory of Weak Processes Involving Neutrinos. II. Pure Leptonic Decays, *Physical Review D* **24**, 1275 (1981).
- [16] New Limits on Heavy Sterile Neutrino Mixing in  $8\text{B}$ -Decay Obtained with the Borexino Detector, *Physical Review D* **88**, 072010 (2013), arXiv:arXiv:1311.5347 [hep-ex].
- [17] J. F. Beacom, S. Chen, J. Cheng, S. N. Doustimotlagh, Y. Gao, G. Gong, H. Gong, L. Guo, R. Han, H.-J. He, X. Huang, J. Li, J. Li, M. Li, X. Li, W. Liao, G.-L. Lin, Z. Liu, W. McDonough, O. Šrámek, J. Tang, L. Wan, Y. Wang, Z. Wang, Z. Wang, H. Wei, Y. Xi, Y. Xu, X.-J. Xu, Z. Yang, C. Yao, M. Yeh, Q. Yue, L. Zhang, Y. Zhang, Z. Zhao, Y. Zheng, X. Zhou, X. Zhu, and K. Zuber, Physics prospects of the Jinping neutrino experiment, *Chinese Physics C* **41**, 023002 (2017), arXiv:1602.01733.
- [18] J. Alwall, R. Frederix, S. Frixione, V. Hirschi, F. Maltoni, O. Mattelaer, H.-S. Shao, T. Stelzer, P. Torrielli, and M. Zaro, The automated computation of tree-level and next-to-leading order differential cross sections, and their matching to parton shower simulations, *Journal of High Energy Physics* **2014**, 1 (2014), arXiv:1405.0301.
- [19] Y. Liang, H. Sun, and Z. Wang, A new tellurium-loaded liquid scintillator based on p-dioxane, arXiv preprint (2025), arXiv:2505.13926.
- [20] W. Shao, W. Xu, Y. Liang, W. Luo, T. Xu, M. Qi, J. Zhang, B. Xu, Z. Wang, and S. Chen, The potential to probe solar neutrino physics with LiCl water solution, *The European Physical Journal C* **83**, 799 (2023), arXiv:2203.01860.